PIER

All-Dielectric Cylindrical Metasurfaces for Enhanced Directional Scattering

Rasmus E. Jacobsen* and Samel Arslanagić

Department of Space Research and Technology, Technical University of Denmark
Bld. 348, Ørsteds Plads, 2800 Kgs. Lyngby, Denmark

ABSTRACT: We present a detailed analytical and numerical study of cylindrical metasurfaces for enhanced scattering applications. Analytical expressions are derived for the surface impedances of single and double metasurface configurations, respectively, which are required to maximize scattering in the forward direction. A surface impedance model is developed for 1-D arrays of dielectric cylinders that is subsequently used to realize and implement numerically the required surface impedances. Our analytical and full-wave numerical results reveal that cylindrical all-dielectric metasurfaces may exhibit superior forward scattering and balanced higher-order mode excitation in comparison to traditional solid dielectric resonators. Two examples, both with silicon dielectric cylinder, have been chosen to showcase our results, and they were found to exhibit extraordinary directional scattering properties with the respective forward scattering efficiencies being 9 and 19 times that of a single mode resonator. The choice of silicon for the cylinder dielectrics highlights the potential of the proposed configuration in optical communications, although the presented theory applies across the other parts of the electromagnetic spectrum.

1. INTRODUCTION

Metasurfaces (MSs) are flat functional structures enabling advanced wave manipulations such as cloaking, perfect absorption, and lasing, to mention a few [1–7]. In particular, all-dielectric MSs have garnered significant interest due to their lower losses at infrared and optical frequencies, unlike their metallic counterparts suffering from ohmic losses. A MS consists of periodic subwavelength unit cells forming a 2-D lattice, typically placed in a rectangular plane. However, recent studies have shown that MSs can also be utilized in cylindrical and spherical shapes as well. Curved surfaces form closed structures, which can be employed for both enhanced and suppressed scattering (cloaking) as well as vortex generation, polarization conversion, and local field enhancement [8–22]. In cylindrical configurations, MSs are often characterized by effective surface impedances or admittances, which can be tailored by adjusting the geometry and material composition of their underlying unit cells. This versatility allows for the realization of nearly any surface impedance/admittance values at desired frequencies, making MSs more adaptable than bulk materials with limited permittivity/permeability values.

For instance, a multilayered cylindrical resonator with superscattering properties was proposed in [23]. The resonator furnishes strong directional scattering by exciting multiple balanced modes, which is often associated with the Huygens source and Kerker's condition utilized in transmitting MSs and directional antennas [24–28]. However, this design requires a combination of materials with specific positive and negative permittivities, making it difficult to realize in practice. Instead,

cascaded MSs, which can achieve similar scattering properties, offer a more feasible solution [9]. Other cylindrical configurations with enhanced scattering have also been proposed, such as an MS imbedded in a high-permittivity material [8] and a corrugated metallic cylinder [29].

Although the underlying theory for cylindrical MSs applies across the electromagnetic spectrum, its primary utilization has been at microwave frequencies. This preference arises from the treatment of MSs as homogenized surfaces with effective surface impedances/admittances which are more common in electrical engineering. Moreover, most analytical surface impedance/admittance models are formulated for printed circuit boards (PCBs) consisting of dielectric substrates with thin metallic elements, which are not particularly suitable for optics [30–32]. However, recent studies have proposed analytical models for MSs of graphene [33–36], as well as plasmonic [13, 37] and dielectric spheres [38, 39] applicable to THz and optical frequencies. The sphere models are available in both simple quasi-static form and more advanced versions including multipolar contributions. These models have shown good agreement with simulations for planar MSs and have also been used to design plasmonic MSs for cloaking cylindrical structures, demonstrating their applicability surfaces [13].

The purpose of the present work is to investigate all-dielectric cylindrical MSs for enhanced directional scattering. While others have studied similar configurations to minimize the total scattering for cloaking applications, our focus is to examine their potential within directive scattering manipulation. Due to the cylindrical configuration, it is more practical to use 1-D model realizations of MSs, as shown in Fig. 1, instead of the 2-D kinds discussed in previous studies [38]. Therefore,

---

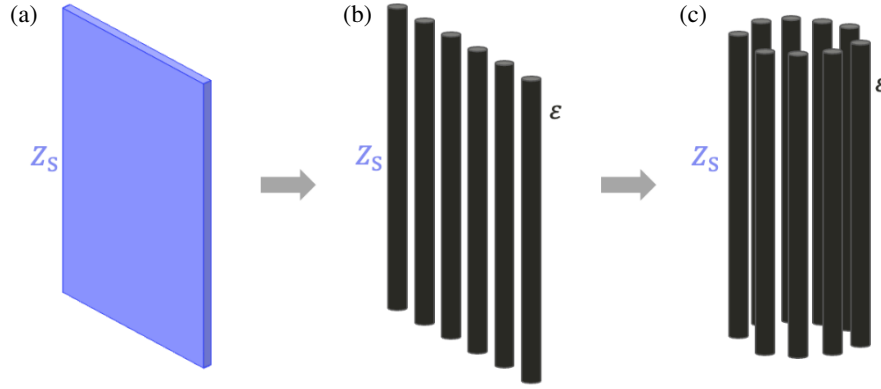* Corresponding author: Rasmus E. Jacobsen (rajac@dtu.dk).

FIGURE 1. Sketch of the (a) homogenized MS, (b) planar 1-D MS and (c) cylindrical 1-D MS.

an analytical surface impedance model is proposed for an MS composed of a 1-D array of high-permittivity dielectric cylinders in a low-permittivity host medium. Operating in the quasi-static regime, this MS can only exhibit a capacitive surface impedance. It has been shown that the resonances are much more prominent in hollow cylindrical MSs with capacitive (inductive) surface impedances for wave incidences with vertical (horizontal) polarization [15, 40]. Consequently, this work focuses solely on vertical polarization.

In this work, the cylindrical MS configuration is treated both analytically and numerically. Analytical expressions for the surface impedance, required to maximize the forward scattering, are derived for resonators with a single and double MSs. The surface impedance model is then used to determine the MS designs. Thus, we obtain a fully analytical design and scattering model for the cylindrical MS configuration. The accuracy of this model is validated by comparing the analytical results with full-wave simulations, showing excellent agreement for MSs with subwavelength unit cells. Additionally, examples demonstrating enhanced forward scattering are presented, showcasing extraordinary scattering performances. The dielectric material in the MSs has a relative permittivity value of 12, corresponding to silicon, indicating their potential in optics. Such optical resonators hold great promise for communication and sensing applications.

The manuscript is structured as follows. The surface impedance model for the 1-D planar MS is first presented and analyzed in Section 2. In Section 3, the scattering properties of cylindrical MS resonators are compared with those of solid dielectric resonators. Moreover, we assess the accuracy of the analytical model for the cylindrical MS resonators by evaluating it against full-wave simulations. The resonators with enhancing forward scattering are then investigated for single and double MSs in Section 4. For both configurations, two examples exhibiting extraordinary directional scattering properties are presented. Throughout this work, the time factor $\exp(j\omega t)$, where ω is the angular frequency and t the time, is assumed and suppressed.

2. METASURFACE CHARACTERIZATION IN TERMS OF A SURFACE IMPEDANCE

As illustrated in Fig. 1, any surface structure, including MSs, can be characterized by an effective surface impedance $Z_{\mathrm{S}} = R_{\mathrm{S}} + jX_{\mathrm{S}}$, where R_{S} and X_{S} represent the surface resistance and reactance, respectively. This surface impedance, whether electric or magnetic kind, can be expressed as [41]

$$Z_{\mathrm{S}} = \frac{\eta_{\mathrm{h}}}{k_0 d_{\mathrm{S}}} \left(\frac{1}{\alpha} - \beta \right) \tag{1}$$

where d_{S} is the lattice constant, η_{h} the intrinsic impedance of the host medium, α the effective normalized electric or magnetic polarizability, and β the normalized interaction constant. In general, Z_{S} and α are tensors, but with the present MSs being operated in the deeply subwavelength regime (quasi-static condition) and the incident wave being polarized along the cylinder axis, both can be treated as scalars. Additionally, only lossless configurations are investigated, implying that $Z_{\mathrm{S}} = jX_{\mathrm{S}}$.

Presently, a planar MS comprising a 1-D array of dielectric cylinders as illustrated in Fig. 2(a) is considered. The MS exhibits a surface impedance as described by (1). The normalized electric polarizability of deeply subwavelength dielectric cylinders is given by $\alpha_{\mathrm{e}}^z = V_{\mathrm{c}}'(\varepsilon - \varepsilon_{\mathrm{h}})/\varepsilon_{\mathrm{h}} d_{\mathrm{S}}^2$, where $V_{\mathrm{c}}' = \pi r_{\mathrm{S}}^2$ is the volume of the cylinder per length, r_S the radius of the cylinders, and ε (ε_{h}) the permittivity of the dielectric cylinder (host medium) [42]. Notably, under vertical polarization (electric field parallel with the cylinder, z-axis, see Fig. 2(a)), we find that there is minimal interaction between the subwavelength cylinders, resulting in $\beta \approx 0$.

As an example, we examine dielectric cylinders with permittivity $\varepsilon = 12\varepsilon_0$ placed in free space ($\varepsilon_{\mathrm{h}} = \varepsilon_0$). In Fig. 2(b), the surface reactance calculated using (1) is shown as a function of the lattice constant for different filling fractions ($r_{\mathrm{S}}/d_{\mathrm{S}}$). Please note that the filling ratio is kept constant for each graph, meaning that the radius r_{S} also changes when d_{S} is changed. To validate the model, the surface reactance was also extracted from the simulated reflection coefficient of the infinite peri-
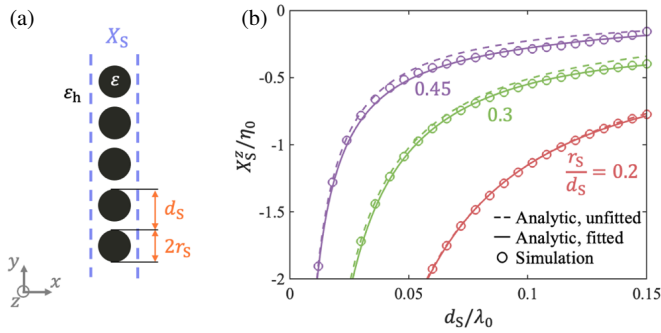
FIGURE 2. Planar MS characterized by an effective surface impedance. (a) Sketch of the MS consisting of a 1-D array of dielectric cylinders. (b) The normalized z-component of the surface reactance as a function of the lattice constant d_S/λ_0, with λ_0 being the free-space wavelength. Each of the graphs is recorded for different filling fractions r_S/d_S. The cylinders have the permittivity $\varepsilon = 12\varepsilon_0$ and the host medium is that of free space ($\varepsilon_h = \varepsilon_0$).

odic array using COMSOL Multiphysics (for details on the extraction method, see e.g., Ref. [38]). The simulation results, shown in Fig. 2(b), are in good agreement with the analytical model. However, for larger cylinders, the dispersion of the array is not fully captured by the simple polarizability model. This limitation is evident for dense arrays ($r_S = 0.45d_S$) in Fig. 2(b). To improve the fit, more advanced polarizability models can be used [38, 39]. However, the deviations between the quasi-static model and the simulation are small in Fig. 2(b), and therefore, a fit function C is introduced to (1) instead, $X_S^{fit} = X_S^{unfit}/C$. A second-degree polynomial correction factor was derived for each filling fraction using a least-squares fit with the simulation results. For $r_S = 0.45d_S$, the correction factor $C = (13.4\,\mathrm{m^{-2}})d_S^2 - (3.43\,\mathrm{m^{-1}})d_S + 1.04$ is used. The results for both the unfitted ($C = 1$) and fitted models are included in Fig. 2(b) depicting a slight improvement with the fitted model.

3. CYLINDRICAL METASURFACE RESONATORS

In the remainder of the work, we focus on cylindrical MSs. The configuration under study is an infinitely long circular cylindrical structure with a radius r, positioned such that the z-axis of the rectangular coordinate system coincides with the cylinder axis. The structure is illuminated by a linearly polarized plane wave propagating in the $+x$-direction. Given the canonical configuration, the internal and scattered fields can be analytically determined using the classical Lorentz-Mie analysis for cylindrical harmonics [43].

Initially, we investigate and compare the scattering properties of a solid dielectric resonator (Case A) and the cylindrical MS resonator composed of unit cells with dielectric cylinders (Case B). Cross-sectional sketches of both resonators are shown in Fig. 3(a). The resonators have the same radius and permittivity. While the solution to the scattered field coefficients of Case A is well known, Case B presents a more complex electromagnetic scattering problem if one attempts to calculate the exact fields. Instead, Case B can be significantly simplified by mod-

eling the MS with an effective surface impedance, Z_S, using (1) on which a surface current density $\mathbf{J}_S = \mathbf{E}_{tan}/Z_S$ is induced with $\mathbf{E}_{tan}$ being the tangential electric field. Thus, the configuration is reduced to an empty cylinder consisting of a cylindrical surface impedance. By applying the impedance boundary condition, $\mathbf{H}_{tan} = \mathbf{E}_{tan}/Z_S$, the analytical solution to the field coefficients is determined. For the vertical polarization, the scattering (field) coefficients are

$$a_n = -\frac{J_n(x_0)^2}{J_n(x_0)^2 + j\left[\frac{2X_S}{\pi\eta_0 x_0} - J_n(x_0)Y_n(x_0)\right]} \quad (2)$$

where $x_0 = k_0 r$, and k_0 and η_0 are the free-space wavenumber and intrinsic impedance, respectively. J_n and Y_n are the Bessel functions of the first and second kinds, respectively, and of order n. The differential and total scattering efficiencies are used to evaluate the scattering from the resonators, determined as $dQ_{sca}(\phi) = (2/x_0)|\sum_{n=-\infty}^{\infty} a_n \exp(jn\phi)|^2$ and $Q_{sca} = (2/x_0)\sum_{n=-\infty}^{\infty} |a_n|^2$, respectively, where ϕ is the polar coordinate.

To compare Case A and Case B, a radius of $r = 0.15\lambda_0$ and a permittivity $\varepsilon = 12\varepsilon_0$ are chosen. For Case B, the MS consists of 16 unit cells with $r_S = 0.45d_S$, and the fitted surface reactance shown in Fig. 2(b) is used to model the MS. The resulting total scattering efficiencies as functions of the normalized frequency are shown in Fig. 3(b). Both resonators exhibit scattering peaks produced by various excited modes. As expected, the dipolar modes ($n = 0$ and 1), having fields more concentrated in the center of the resonator, are more efficiently excited in the solid dielectric resonator (Case A). However, for higher-order modes, the cylindrical MS (Case B) shows superior performance. This is confirmed by the full-wave simulation of the near fields of the two resonators, shown in Fig. 3(c) for the electric quadrupolar mode ($n = 2$). Notably, the cylindrical MS demonstrates a much stronger forward scattering response, making it highly suitable for transmission applications. This prominent feature will be investigated further in Section 4, but first we want to investigate the validity of the proposed analytical model.

The inhomogeneity and curvature of the MS is not considered with the analytical model, and thus some inaccuracies are expected. This is analyzed in Fig. 4, which shows the total scattering efficiency as a function of the radius and the number of unit cells (N_S). As in Fig. 3 (Case B), the permittivity is $\varepsilon = 12\varepsilon_0$ and $r_S = 0.45d_S$. The results from full-wave simulations are included, showing overall good agreement with the analytical model. Particularly, MSs with more unit cells, forming more homogeneous surfaces, exhibit excellent match. As the number of unit cells decreases, the analytical model becomes less accurate.

Besides indicating the accuracy of the analytical model, Fig. 4 also illustrates how the MS can be engineered for specific scattering responses by simply changing the geometrical parameters of the MS. This flexibility is a significant advantage as most canonical resonators offer very few tuning parameters.
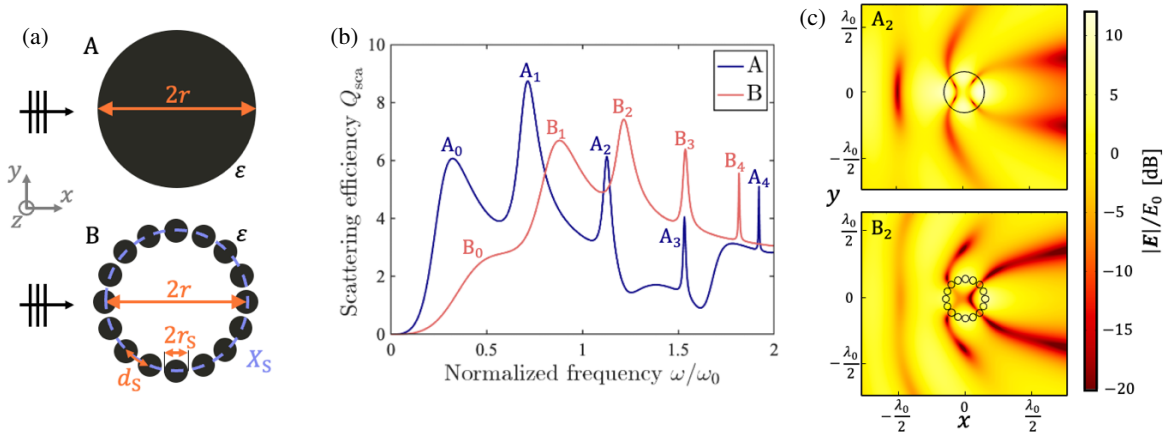
FIGURE 3. Solid dielectric cylinder (A) and cylindrical MS (B) resonators. (a) Cross-sectional sketch of the resonators and (b) the scattering efficiency as a function of the normalized frequency. The radius $r = 0.15\lambda_0$ and the permittivity is $\varepsilon = 12\varepsilon_0$. The MS contains 16 unit cells with $r_S = 0.45d_S$. (c) Electric field magnitude (logarithmic scale) in the xy-plane obtained from full-wave simulations.
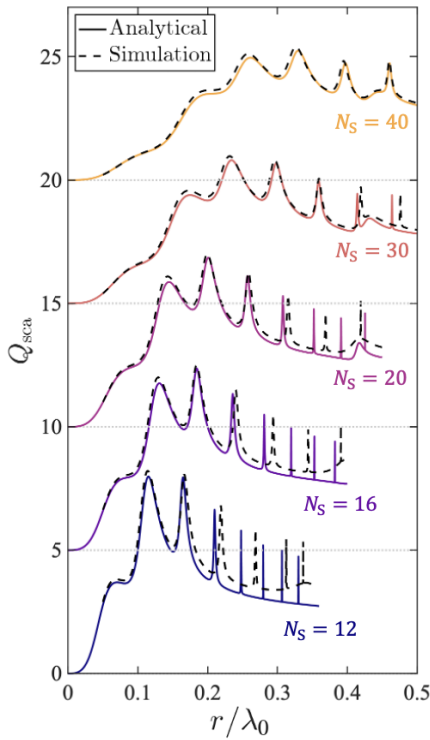

FIGURE 4. Comparison of the analytical model and full-wave simulation of the cylindrical MS resonator. Scattering efficiency as a function of the radius for different number of unit cells N_S with $r_S = 0.45d_S$. The calculations are limited up to maximum mode $n = 7$, and the vertical axis is shifted by 5 for each graph.

4. ENHANCED DIRECTIONAL SCATTERING

In this section, we illustrate the advantages of cylindrical metasurfaces (MSs) for enhancing the forward scattering. This enhancement is achieved by exciting multiple modes, a concept that has been explored in various structures [24–28]. The challenge lies in balancing these modes by considering both their amplitudes and phases, obtaining states sometimes referred to as Kerker's condition or Huygens source effect [24]. Ini-

tially, this condition was applied only to dipolar modes but has since been generalized to other multipoles [25]. Our goal is to maximize the forward scattering, specifically $dQ_{\text{sca}}(\phi = 0°) = (2/x_0)|\sum_{n=-\infty}^{\infty} a_n|^2$. Given that $a_n = -1$ for a resonant mode, this condition is also necessary for all combined modes and differs from maximizing the total scattering efficiency Q_{sca}, where just $|a_n| = 1$ is required. However, it is important to note that both scattering efficiencies are maximized when $a_n = -1$. In this case, the scattering efficiencies are maximized to $dQ_{\text{sca}}(\phi = 0°) = (2/x_0)(2N + 1)^2$ and $Q_{\text{sca}} = (2/x_0)(2N + 1)$, where N is the number of modes excited, beside the $n = 0$ mode. If the $n = 0$ mode is not excited, the theoretical maxima are $dQ_{\text{sca}}(\phi = 0°) = (2/x_0)(4N^2)$ and $Q_{\text{sca}} = (2/x_0)(2N)$.

From (2), it is straightforward to determine that $a_n = -1$ when

$$X_S = \eta_0 \frac{\pi x_0 J_n(x_0) Y_n(x_0)}{2} \tag{3}$$

To excite two modes (n and m) with $X_S^n = X_S^m$, we require $J_n(x_0)Y_n(x_0) = J_m(x_0)Y_m(x_0)$, necessitating specific sizes and surface reactances. This constrain is confirmed in Fig. 5(a), where the required surface reactances for modes 0 up to 4 as functions of the radius are shown. The intersection points on the graphs indicate designs where the resonances of two modes overlap. Fortunately, mostly capacitive surfaces are needed, allowing the use of the MSs from Fig. 2.

To demonstrate that these resonators indeed maximize forward scattering, we selected two designs: Design A, combining modes $n = 0$ and 1, and Design B, combining modes $n = 1$ and 2. The required surface reactance $X_S = -0.30\eta_0$ ($X_S = -0.54\eta_0$) is achieved with the MS design parameters $r = 0.086\lambda_0$ ($0.245\lambda_0$), $N_S = 6$ (33) and $r_S = 0.45d_S$ ($0.45d_S$) for Design A (Design B). The simulated local electric field (colors) and power flow density (arrows), shown in Fig. 5(b), reveal a significant forward scattering compared to the backward scattering. This is further confirmed by the normalized differential scattering efficiency $dQ_{\text{sca,n}}(\phi) = (x_0/2)dQ_{\text{sca}}(\phi)$ depicted in Fig. 5(c). The expected scattering patterns are observed, with
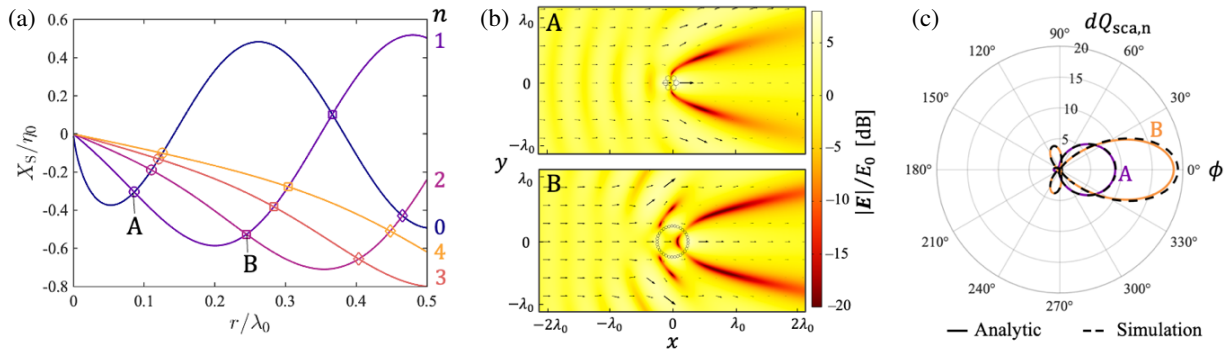
FIGURE 5. Enhancing directional scattering with a single-MS resonator. (a) Required surface reactance as a function of the radius for modes $n = 0, 1, 2, 3$ and 4 calculated using (3). (b) Simulated local electric field magnitude (colors, logarithmic scale) and power flow density (arrows, linear scale) in the xy-plane for Design A and B highlighted in (a). (c) The analytical and simulated normalized differential scattering efficiency $dQ_{\text{sca,n}}(\phi)$. The excited modes are $n = 0, 1$ (Design A) and $n = 1, 2$ (Design B). The design parameters are $r = 0.086\lambda_0$ ($0.245\lambda_0$), $N_{\text{S}} = 6$ (33) and $r_{\text{S}} = 0.45d_{\text{S}}$ ($0.45d_{\text{S}}$) for Design A (B).

Design A achieving the theoretical maximum of 9 and Design B slightly exceeding the theoretical maximum of 16 due to a minor contribution coming from the $n = 0$ mode. To further enhance the scattering, more modes must be excited.

For a single MS design as the one studied in Fig. 5, incorporating more modes entails larger resonators. However, recent studies have shown that cascading cylindrical MSs can further enhance the total scattering [9, 17]. The single-layer design analyzed in Figs. 4 and 5 is fundamentally limited by the lack of multiple overlapping modes according to (2), prompting us to extend our design to include an additional MS. A double MS resonator presents a more complex configuration, leading to more intricate solutions for the field coefficients. However, this intricacy also significantly expands the design possibilities as we will illustrate in the next part.

The new resonator design consists of two concentric cylindrical MSs with the radius and surface reactance of the inner (outer) MSs being denoted r_1 (r_2) and X_{S1} (X_{S2}), respectively. The cylinder core and the layer between the MSs are empty and are modelled as free space. The derivation of the analytical solution to the scattering coefficient for the double MS configuration follows the same approach as for the single MS. The solution to the scattering coefficient is given in the Appendix.

Overlapping modes (n and m) are investigated by imposing $a_n = a_m = -1$ and the conditions $X_{\text{S1}}^n = X_{\text{S1}}^m$ and $X_{\text{S2}}^n = X_{\text{S2}}^m$. The solutions to the surface reactances are

$$b_2 \left(\frac{2X_{\text{S1}}}{\pi\eta_0 x_1} \right)^2 + b_1 \frac{2X_{\text{S1}}}{\pi\eta_0 x_1} + b_0 = 0 \tag{4a}$$

$$X_{\text{S2}} = \eta_0 \frac{\pi x_2}{2} \frac{J_n(x_2)Y_n(x_2)\left[J_n(x_1)Y_n(x_1) - \frac{2X_{\text{S1}}}{\pi\eta_0 x_1} \right]}{-J_n(x_1)^2 Y_n(x_2)^2} \frac{}{J_n(x_1)Y_n(x_1) - \frac{2X_{\text{S1}}}{\pi\eta_0 x_1}} \tag{4b}$$

where $x_1 = k_0 r_1$ and $x_2 = k_0 r_2$. The coefficients b_2, b_1, and b_0 in (4a) are provided in the Appendix. From (4), two solutions can be obtained for each mode combination and all values of r_1 and r_2. The presented results are limited to the

mode combination $n = 0, 1$, shown in Fig. 6. The surface reactances (colors) are depicted as function of the radii in Figs. 6(a)–(d), whereas the resulting $dQ_{\text{sca,n}}(0)$ is shown in Figs. 6(e) and (f). The white spaces denote the complex solutions to the surface reactances coming from the quadratic equation in Eq. (4a). These solutions correspond to active surface designs ($R_{\text{S}} < 0$), and thus these solutions have been omitted. The colors in Figs. 6(a)–(d) indicate the surface reactance being either capacitive (red) or inductive (blue). The theoretical minimum of $dQ_{\text{sca,n}}(0) = (1 + 2)^2 = 9$ is confirmed in Figs. 6(e) and (f). It is observed that much higher values of $dQ_{\text{sca,n}}(0)$ can be achieved with some resonator designs coming from the scattering contribution of other excited modes. Eq. (4) ensures that at least two modes are excited, but there is no restriction to the excitation of additional modes. However, it must be noted that for resonators with highly subwavelength radii, the maximum $dQ_{\text{sca,n}}(0)$ is around 9. To further enhance the scattering from such small resonators, additional MSs are needed [9].

Two designs (Designs A and B) exhibiting particularly strong forward scattering have been selected and are marked in Fig. 6. The analytical $dQ_{\text{sca,n}}(0)$ is around 37 and 75 for Designs A and B, respectively. These superscattering properties are coming from the excitation of not only the $n = 0$ and 1 modes, but also a partial excited mode ($n = 2$) and a nearly fully excited mode ($n = 3$) for Design A. For Design B, additional modes $n = 2$, 3, and 4 are close to being fully excited. All the MSs have surface reactances achievable with the MS design proposed in Section 2. For Design A, the required surface reactances $X_{\text{S1}} = -0.85\eta_0$ ($X_{\text{S2}} = -0.39\eta_0$) are achieved with the MS design parameters $r_1 = 0.40r_2$ ($r_2 = 0.29\lambda_0$) and $N_{\text{S1}} = 26$ ($N_{\text{S2}} = 27$) for the inner (outer) MS. For Design B, the required surface reactances $X_{\text{S1}} = -0.93\eta_0$ ($X_{\text{S2}} = -0.85\eta_0$) are obtained with $r_1 = 0.56r_2$ ($r_2 = 0.50\lambda_0$) and $N_{\text{S1}} = 69$ ($N_{\text{S2}} = 83$) for the inner (outer) MS. The filling ratio remains $r_{\text{S}} = 0.45d_{\text{S}}$ for all MSs. The simulated local electric field intensity and power flow density, as well as the far-field parameter $dQ_{\text{sca,n}}(\phi)$, shown in Fig. 7, confirm the enhanced directional scattering resulting from the multimode excitation in both resonators. Compared to a single-mode resonator (as-
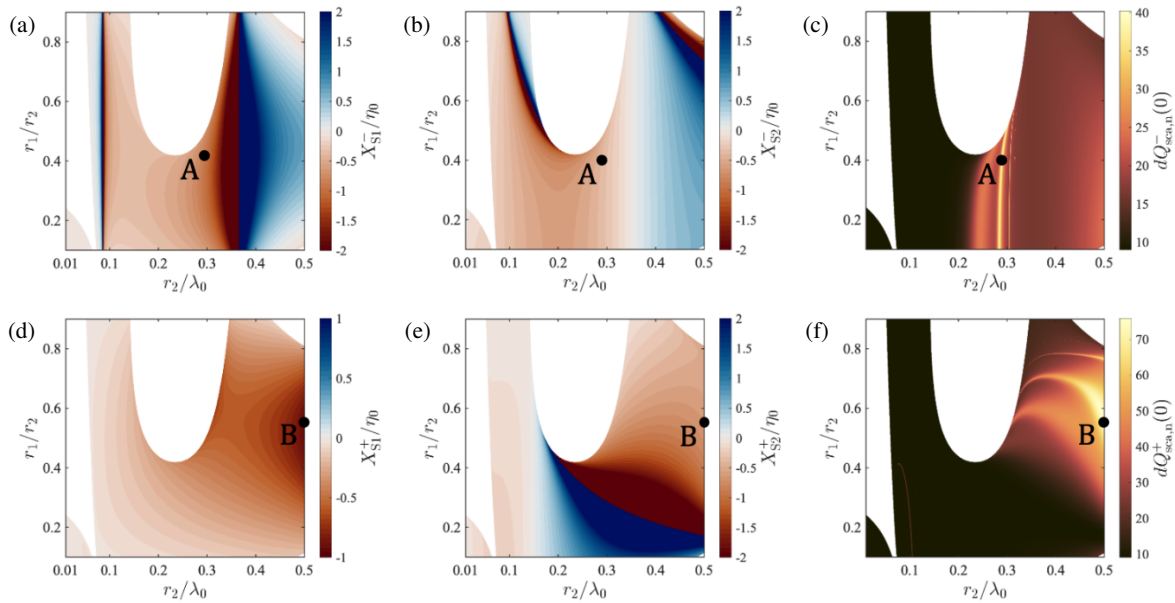
FIGURE 6. Enhancing directional scattering with a double MS resonator fully exciting the $n = 0$ and 1 modes. The surface reactance (colors) of the inner [(a), (b)] and outer [(c), (d)] MSs as a function of r_2/λ_0 and r_1/r_2. The resulting normalized differential scattering efficiency in the forward direction $dQ_{\mathrm{sca,n}}(0)$ is shown in (e) and (f). The top (bottom) panel show the — (+) solution of (4). The two highlighted designs (Design A and B) are further analyzed in Fig. 7.
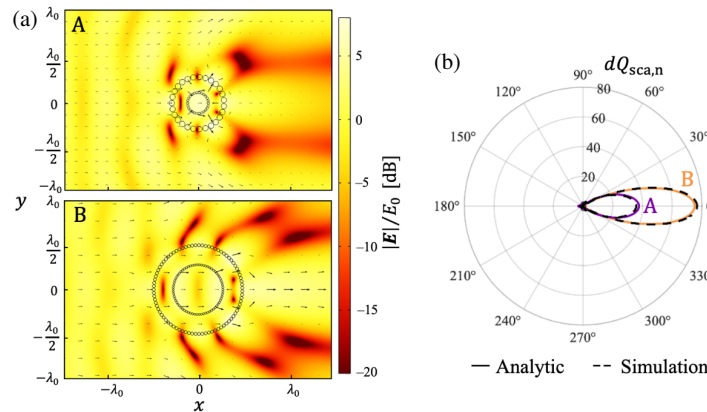

FIGURE 7. Two examples of double MS resonators with enhancing directional scattering. Simulated local electric field magnitude (colors, logarithmic scale) and power flow density (arrows, linear scale) in the xy-plane for Design A and B, which are marked in Fig. 6. (b) The analytical and simulated normalized differential scattering efficiency $dQ_{\mathrm{sca,n}}(\phi)$. The surface reactances and the design parameters for the MSs are provided in the text.

suming that the excited mode is $n \geq 1$), the forward (total) scattering efficiencies are around 9 and 19 (3 and 4) times for Designs A and B, respectively. Additionally, the minor scattering lobes are well suppressed being 12.1 dB (Design A) and 13.5 dB (Design B) below the major lobe.

Various multimode cylindrical resonators have been previously reported, but differences in size, material, and excitation make direct comparison difficult [8, 9, 20, 23, 29, 44, 45]. Electrically small resonators with high scattering efficiencies rely on extreme permittivities but are highly sensitive to material and size changes. Larger resonators, like our Design B in Fig. 7, offer comparable efficiency with greater practicality. Our designs stand out by using moderate, realistic permittivity values, making them suitable for infrared and optical frequencies.

5. CONCLUSIONS

In this study, cylindrical MS resonators were analyzed both analytically and numerically. A surface impedance model was developed for a 1-D array of dielectric cylinders operating under vertical polarization and in the quasi-static regime. The model was then coupled to the analytical solution for cylindrical MSs resulting in a comprehensive analytical framework demonstrating good agreement with careful full-wave simulations.

The scattering of a solid dielectric resonator was compared to that of a cylindrical MS, demonstrating that the latter is more favorable for higher-order mode excitation. Moreover, due to their engineerable surface impedance, cylindrical MSs offer superior control over balanced higher-order mode excitation,

thereby maximizing forward scattering compared to traditional solid dielectric resonators. Analytical expressions for the required surface impedance to maximize forward scattering were derived for resonators with both single and double MSs. Examples presented in this work highlighted extraordinary directional scattering performances resulting from the excitation of multiple modes.

All calculations utilized a relative permittivity of 12, corresponding to silicon, indicating the potential applications of these MSs within optical communication and sensing. The straightforward design and material composition of the proposed MS resonator make it significantly simpler than many other resonator structures, allowing it to serve as a potential substitute for numerous existing designs. A promising extension of this work involves incorporating gain materials into the resonators to further enhance their total scattering. Moreover, tunable materials can be utilized to make the scattering reconfigurable possibly enabling beam steering capabilities. At last, the presented theory and examples are not limited to optics only and can be applied across different parts of the electromagnetic spectrum.

APPENDIX A.

The scattering coefficients for the cylindrical double MS resonator under TM polarization are given by

$$a_n^{2\mathrm{MS}} = -\frac{J_n(x_2)\left[Y_n(x_2) - K_n J_n(x_2)\right] + \frac{2X_{S2}}{\pi \eta_0 x_2}}{J_n(x_2)\left[Y_n(x_2) - K_n J_n(x_2)\right] + \frac{2X_{S2}}{\pi \eta_0 x_2}} -j\left[\frac{2X_{S2}}{\pi \eta_0 x_2} K_n + Y_n(x_2)^2 - K_n J_n(x_2) Y_n(x_2)\right]$$
(A1a)

where

$$K_n = \frac{J_n(x_1) Y_n(x_1) - \frac{2X_{S1}}{\pi \eta_0 x_1}}{J_n(x_1)^2}$$
(A1b)

The expressions for the coefficients in (4) are

$$b_2 = J_m(x_2) Y_m(x_2) - J_n(x_2) Y_n(x_2)$$
(A2a)

$$b_1 = \left[J_m(x_1) Y_m(x_2)\right]^2 - \left[J_n(x_1) Y_n(x_2)\right]^2 \\ -b_2\left[J_m(x_1) Y_m(x_1) + J_n(x_1) Y_n(x_1)\right]$$
(A2b)

$$b_0 = J_m(x_1) J_n(x_1)\left[b_2 Y_m(x_1) Y_n(x_1) \\ +J_n(x_1) Y_m(x_1) Y_n(x_2)^2 \\ -J_m(x_1) Y_n(x_1) Y_m(x_2)^2\right]$$
(A2c)

REFERENCES

[1] Zografopoulos, D. C. and O. Tsilipakos, "Recent advances in strongly resonant and gradient all-dielectric metasurfaces," *Materials Advances*, Vol. 4, No. 1, 11–34, 2023.

[2] Jacobsen, R. E., S. Arslanagić, and A. V. Lavrinenko, "Water-based devices for advanced control of electromagnetic waves," *Applied Physics Reviews*, Vol. 8, No. 4, 041304, 2021.

[3] Zahra, S., L. Ma, W. Wang, J. Li, D. Chen, Y. Liu, Y. Zhou, N. Li, Y. Huang, and G. Wen, "Electromagnetic metasurfaces and reconfigurable metasurfaces: A review," *Frontiers in Physics*, Vol. 8, 593411, 2021.

[4] Glybovski, S. B., S. A. Tretyakov, P. A. Belov, Y. S. Kivshar, and C. R. Simovski, "Metasurfaces: From microwaves to visible," *Physics Reports*, Vol. 634, 1–72, 2016.

[5] Overvig, A. and A. Alù, "Diffractive nonlocal metasurfaces," *Laser & Photonics Reviews*, Vol. 16, No. 8, 2100633, 2022.

[6] Grbic, A. and S. Maci, "EM metasurfaces [Guest Editorial]," *IEEE Antennas and Propagation Magazine*, Vol. 64, No. 4, 16–22, 2022.

[7] Jahani, S. and Z. Jacob, "All-dielectric metamaterials," *Nature Nanotechnology*, Vol. 11, No. 1, 23–36, 2016.

[8] Jacobsen, R. E., A. V. Lavrinenko, and S. Arslanagić, "Reconfigurable dielectric resonators with imbedded impedance surfaces — From enhanced and directional to suppressed scattering," *Applied Physics Letters*, Vol. 122, No. 8, 081701, 2023.

[9] Qian, C., X. Lin, Y. Yang, X. Xiong, H. Wang, E. Li, I. Kaminer, B. Zhang, and H. Chen, "Experimental observation of superscattering," *Physical Review Letters*, Vol. 122, No. 6, 063901, 2019.

[10] Alù, A., "Mantle cloak: Invisibility induced by a surface," *Physical Review B — Condensed Matter and Materials Physics*, Vol. 80, No. 24, 245115, 2009.

[11] Monti, A., J. C. Soric, A. Alù, A. Toscano, and F. Bilotti, "Anisotropic mantle cloaks for TM and TE scattering reduction," *IEEE Transactions on Antennas and Propagation*, Vol. 63, No. 4, 1775–1788, 2015.

[12] Younesiraad, H., Z. Hamzavi-Zarghani, and L. Matekovits, "Invisibility utilizing Huygens' metasurface based on mantle cloak and scattering suppression phenomen," *IEEE Transactions on Antennas and Propagation*, Vol. 69, No. 8, 5181–5186, 2021.

[13] Monti, A., F. Bilotti, and A. Toscano, "Optical cloaking of cylindrical objects by using covers made of core-shell nanoparticles," *Optics Letters*, Vol. 36, No. 23, 4479–4481, 2011.

[14] Padooru, Y. R., A. B. Yakovlev, P.-Y. Chen, and A. Alù, "Analytical modeling of conformal mantle cloaks for cylindrical objects using sub-wavelength printed and slotted arrays," *Journal of Applied Physics*, Vol. 112, No. 3, 034907, 2012.

[15] Jacobsen, R. E. and S. Arslanagić, "Extreme localization of fields in open cylindrical impedance surface cavities," *IEEE Transactions on Antennas and Propagation*, Vol. 72, No. 2, 1686–1693, 2024.

[16] Lin, C.-W. and A. Grbic, "A realistic coaxial feed for cascaded cylindrical metasurfaces," *IEEE Antennas and Wireless Propagation Letters*, Vol. 22, No. 11, 2624–2628, 2023.

[17] Lin, C.-W. and A. Grbic, "Analysis and synthesis of cascaded cylindrical metasurfaces using a wave matrix approach," *IEEE Transactions on Antennas and Propagation*, Vol. 69, No. 10, 6546–6559, 2021.

[18] Dugan, J., J. G. N. Rahmeier, T. J. Smy, and S. Gupta, "Field scattering analysis of cylindrical spatially dispersive metasurfaces," *IEEE Antennas and Wireless Propagation Letters*, Vol. 22, No. 11, 2619–2623, 2023.

[19] Lin, C.-W. and A. Grbic, "Field synthesis with azimuthally varying, cascaded, cylindrical metasurfaces using a wave matrix approach," *IEEE Transactions on Antennas and Propagation*, Vol. 71, No. 1, 796–808, 2023.

[20] Sipus, Z., M. Bosiljevac, and A. Grbic, "Modelling cascaded cylindrical metasurfaces using sheet impedances and a transmission matrix formulation," *IET Microwaves, Antennas & Propagation*, Vol. 12, No. 7, 1041–1047, 2018.

[21] Šipuš, Z., D. Barbarić, and M. Bosiljevac, "Design of cascaded cylindrical metasurfaces using resonance cancellation method," *IEEE Antennas and Wireless Propagation Letters*, Vol. 22, No. 12, 2841–2845, 2023.

[22] Brugnolo, P., S. Arslanagić, and R. E. Jacobsen, "Bound states in the continuum in cylindrical all-dielectric metasurface cavities," *Physical Review Letters*, Vol. 134, No. 9, 092902, 2025.

[23] Arslanagić, S. and R. W. Ziolkowski, "Highly subwavelength, superdirective cylindrical nanoantenna," *Physical Review Letters*, Vol. 120, No. 23, 237401, 2018.

[24] Ziolkowski, R. W., "Using Huygens multipole arrays to realize unidirectional needle-like radiation," *Physical Review X*, Vol. 7, No. 3, 031017, 2017.

[25] Alaee, R., R. Filter, D. Lehr, F. Lederer, and C. Rockstuhl, "A generalized Kerker condition for highly directive nanoantennas," *Optics Letters*, Vol. 40, No. 11, 2645–2648, 2015.

[26] Jacobsen, R. E., A. V. Lavrinenko, and S. Arslanagić, "A water-based Huygens dielectric resonator antenna," *IEEE Open Journal of Antennas and Propagation*, Vol. 1, 493–499, 2020.

[27] Rahimzadegan, A., D. Arslan, D. Dams, A. Groner, X. Garcia-Santiago, R. Alaee, I. Fernandez-Corbaton, T. Pertsch, I. Staude, and C. Rockstuhl, "Beyond dipolar Huygens' metasurfaces for full-phase coverage and unity transmittance," *Nanophotonics*, Vol. 9, No. 1, 75–82, 2020.

[28] Tang, M.-C., Z. Wu, T. Shi, and R. W. Ziolkowski, "Dual-band, linearly polarized, electrically small huygens dipole antennas," *IEEE Transactions on Antennas and Propagation*, Vol. 67, No. 1, 37–47, 2019.

[29] Shcherbinin, V. I., V. I. Fesenko, T. I. Tkachova, and V. R. Tuz, "Superscattering from subwavelength corrugated cylinders," *Physical Review Applied*, Vol. 13, No. 2, 024081, 2020.

[30] Sievenpiper, D. F., *Artificial Impedance Surfaces for Antennas*, 737–777, Modern Antenna Handbook, 2007.

[31] Simovski, C. R., P. de Maagt, and I. V. Melchakova, "High-impedance surfaces having stable resonance with respect to polarization and incidence angle," *IEEE Transactions on Antennas and Propagation*, Vol. 53, No. 3, 908–914, 2005.

[32] Luukkonen, O., C. Simovski, G. Granet, G. Goussetis, D. Lioubtchenko, A. V. Raisanen, and S. A. Tretyakov, "Simple and accurate analytical model of planar grids and high-impedance surfaces comprising metal strips or patches," *IEEE Transactions on Antennas and Propagation*, Vol. 56, No. 6, 1624–1632, 2008.

[33] Dragoman, M., M. Aldrigo, A. Dinescu, D. Dragoman, and A. Costanzo, "Towards a terahertz direct receiver based on graphene up to 10 THz," *Journal of Applied Physics*, Vol. 115, No. 4, 044307, 2014.

[34] Xiong, H., M.-C. Tang, Y.-H. Peng, Y.-H. Zhong, and X.-H. Tan, "Surface impedance of metasurfaces/graphene hybrid structures," *Nanoscale Research Letters*, Vol. 14, 1–8, 2019.

[35] Fallahi, A. and J. Perruisseau-Carrier, "Design of tunable biperiodic graphene metasurfaces," *Physical Review B — Condensed Matter and Materials Physics*, Vol. 86, No. 19, 195408, 2012.

[36] Monti, A., S. H. Raad, Z. Atlasbaf, A. Toscano, and F. Bilotti, "Maximizing the forward scattering of dielectric nanoantennas through surface impedance coatings," *Optics Letters*, Vol. 47, No. 10, 2386–2389, 2022.

[37] Monti, A., A. Alù, A. Toscano, and F. Bilotti, "Optical invisibility through metasurfaces made of plasmonic nanoparticles," *Journal of Applied Physics*, Vol. 117, No. 12, 123103, 2015.

[38] Monti, A., A. Alù, A. Toscano, and F. Bilotti, "Surface impedance modeling of all-dielectric metasurfaces," *IEEE Transactions on Antennas and Propagation*, Vol. 68, No. 3, 1799–1811, 2020.

[39] Monti, A., A. Alù, A. Toscano, and F. Bilotti, "Design of high-Q passband filters implemented through multipolar all-dielectric metasurfaces," *IEEE Transactions on Antennas and Propagation*, Vol. 69, No. 8, 5142–5147, 2021.

[40] Jacobsen, R. E., A. V. Lavrinenko, and S. Arslanagić, "Scattering properties of high-permittivity dielectric resonators embedded with impedance sheets," in *2022 3rd URSI Atlantic and Asia Pacific Radio Science Meeting (AT-AP-RASC)*, 1–4, Gran Canaria, Spain, 2022.

[41] Tretyakov, S., *Analytical Modeling in Applied Electromagnetics*, Artech House, 2003.

[42] Noguez, C., "Surface plasmons on metal nanoparticles: The influence of shape and physical environment," *The Journal of Physical Chemistry C*, Vol. 111, No. 10, 3806–3819, 2007.

[43] Bohren, C. F. and D. R. Huffman, *Absorption and Scattering of Light by Small Particles*, 1st ed., John Wiley & Sons, Hoboken, New York, 1983.

[44] Beneck, R. J., L. Kang, R. P. Jenkins, S. D. Campbell, and D. H. Werner, "Superscattering of electromagnetic waves from subwavelength dielectric structures," *Optics Express*, Vol. 32, No. 11, 19410–19423, 2024.

[45] Chen, W., B. Lv, J. Fu, T. Jiang, and Y. Li, "Mode-based superdirective optimization strategy for multi-layered dielectric cylinder," *IEEE Transactions on Antennas and Propagation*, Vol. 72, No. 5, 4510–4523, 2024.